第 54 卷第 4 期
2026 年 4 月

硅 酸 盐 学 报
JOURNAL OF THE CHINESE CERAMIC SOCIETY

Vol. 54，No. 4
April，2026

http://jccsoc.cbpt.cnki.net

DOI：10.14062/j.issn.0454-5648.20250630

综 合 评 述

具有法拉第效应的氧化物玻璃的研究进展

TANAKA Katsuhisa

(京都大学工学研究科物质化学系，京都府西京区 615-8510，日本)

摘　要：法拉第效应是指线偏振光穿过磁性材料后，转变为偏振面绕光的传播矢量发生旋转的椭圆偏振光的现象。偏振面的旋转角度——法拉第旋转角(θ)是衡量磁性材料能否应用于电流传感器、磁场传感器、光隔离器及光环行器等器件的关键参数。富含稀土离子的氧化物玻璃具有显著的法拉第效应，尤其在可见光至紫外光波段表现突出，且其磁化强度低于钇铁石榴石($Y_3Fe_5O_{12}$)等铁磁或亚铁磁氧化物晶体(这类晶体已被有效用作光通信领域的光隔离器)。但在可见光至紫外光波段，这类玻璃的透光率显著优于铁基氧化物晶体，而透光率与法拉第旋转角(θ)对材料的实际应用同等重要。本文综述了高法拉第旋转角(θ)氧化物玻璃的最新研究进展，重点关注含稀土元素的相关材料体系，如具有反常铁磁性的氧化铕基非晶氧化物，以及通过无容器工艺制备的富含顺磁性三价铽离子(Tb^{3+})的氧化物玻璃。

关键词：氧化物玻璃；法拉第效应；费尔德常数；铁磁性非晶氧化物；稀土元素；二价铕
中图分类号：J527.3　　**文献标志码**：A　　**文章编号**：0454–5648(2026)04–1307–17
网络出版时间：2026–01–26

1　Introduction

The Faraday effect is a magneto-optical phenomenon observed when linearly polarized light is incident on a magnetic material with the propagation direction of the light parallel to the magnetization or the external magnetic field. As illustrated in Fig. 1, the linearly polarized light is converted into elliptically polarized light, and the main axis-containing polarization plane of the latter light is rotated around the propagation vector with respect to the polarization plane of the former light by a certain angle, the Faraday rotation angle (θ).

From a microscopic point of view, the Faraday effect is ascribed to the differing effects of the absorption of right and left circularly polarized light on single-spin excitation in the presence of magnetization or external magnetic field (Fig. 2) [1]. Here, it should be noted that linearly polarized light is a combination of right and left circularly polarized light. The excited state is split into two levels because of spin–orbit coupling. Owing to the conservation of angular momentum, right and left

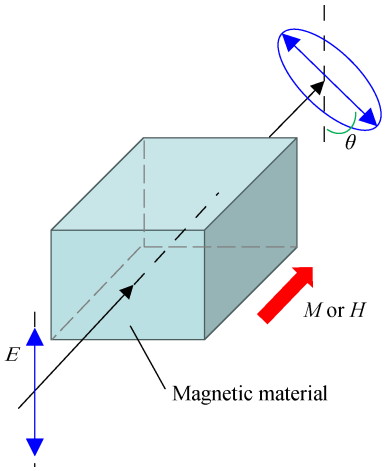

Note: E, M, H, and θ denote the electric field vector of linearly and elliptically polarized light, magnetization, external magnetic field, and Faraday rotation angle, respectively. The propagation direction of linearly polarized light is parallel to the direction of magnetization or external magnetic field.

Fig. 1　Schematic explaining the Faraday effect

circularly polarized light excites the spin into the states with orbital angular momentum L = +1 and −1, respectively. Consequently, the optical absorption spectrum (and hence, the wavelength dependence of the

收稿日期：2025–08–26。　修订日期：2025–09–30。
基金项目：Nippon Electric Glass Co., Ltd。
第一作者：TANAKA Katsuhisa (1961—)，男，教授。

Received date: 2025–08–26.　**Revised date:** 2025–09–30.
First author: TANAKA Katsuhisa (1961–), male, Professor.
E-mail: tanaka.katsuhisa.4n@kyoto-u.ac.jp

refractive index) for right circularly polarized light is different from that for left circularly polarized light. The difference in the refractive index gives rise to a phase difference between right and left circularly polarized light, leading to polarization plane rotation, while the difference in absorption between right and left circularly polarized light causes elliptical polarization.

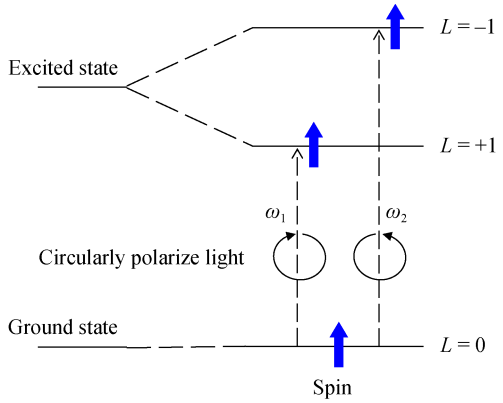

Note: Owing to the conservation of angular momentum, right and left circularly polarized light develop different wavelength dependences of absorption and refractive-index, leading to the Faraday effect.

Fig. 2 Schematic energy level diagram and excitation process of a single spin in the presence of magnetization or an external magnetic field

The Faraday effect is used in electric-current and magnetic-field sensors, optical circulators, and optical isolators. The effective operation of magnetic material–based devices simultaneously requires high θ and transmittance. Thus, the magneto-optical figure of merit for the Faraday effect is defined as θ divided by absorbance.

Magnetic materials exhibiting large Faraday effects include garnet-type ferrites such as $Y_3Fe_5O_{12}$ (yttrium iron garnet, YIG) and $Gd_3Fe_5O_{12}$ (GIG) [2–3]. Bi-substituted YIG and GIG are used as isolators in optical telecommunications utilizing silica glass fiber as an information transmission medium because of their very low absorbance and large θ in the optical-signal wavelength range (1.3–1.5 μm). However, owing to the presence of Fe^{3+}, garnet-type ferrites strongly absorb in the visible to ultraviolet light.

Optical isolators are important devices for telecommunications and high-power laser technology. In many optical systems, light reflection can fatally damage the light source, especially in high-power laser systems, and should therefore be avoided. Hence, optical isolators efficiently operating in a wide wavelength range, particularly in the short-wavelength region not covered by garnet-type ferrites, are in high demand. Magnetic semiconductors hold promise in this regard[4–6], *e.g.*, $Cd_{0.24}Mn_{0.76}Te$ thin film epitaxially grown on sapphire substrate using an ionized-cluster beam method exhibits large Faraday effect at an incident photon energy corresponding to the band gap of the thin film [6]. The corresponding magneto-optical figure of merit (400 deg) is sufficiently large for application to an optical isolator in a photon energy range of 1.8–1.9 eV (corresponding to a wavelength range of 650–690 nm) at room temperature when an external field of 5 kOe is applied.

Rare earth–rich oxide crystals and glasses also effectively operate in the visible to ultraviolet range. A notable example is $Tb_3Ga_5O_{12}$ (TGG), which adopts the garnet-type structure similarly to YIG and GIG and is used in singe-crystalline form as a commercial optical-isolator component[7]. The abundant Tb^{3+} ions give rise to large θ, especially at short wavelengths. The Faraday effect in oxide glasses rich in rare-earth ions has been extensively explored since the 1960s[8–10]. From the viewpoint of practical applications, oxide glasses can be processed into large specifically shaped substrates and composition-tuned to achieve optimized magneto-optical characteristics and are therefore superior to single-crystalline oxides such as TGG.

The present paper reviews the Faraday effect in oxide glasses (mostly of diamagnetic or paramagnetic origin) at room temperature. The examined paramagnetic glasses are mainly those rich in rare-earth ions, in which case Faraday rotation is usually due to 4f–5d transitions. Particular focus is placed on Eu^{2+}-containing oxide glasses and amorphous thin films undergoing ferromagnetic phase transitions. Tb^{3+}-containing glasses prepared by containerless processing and exhibiting θ values exceeding those of oxide glasses obtained by conventional melt quenching are also described, and several examples of oxide glasses containing 3d transition metal ions are mentioned. In addition, the Faraday effect in glass-ceramics featuring nanocrystals embedded in a transparent glass matrix is discussed.

2 Faraday effect in diamagnetic oxide glasses

The Faraday effect, discovered by Michael Faraday in lead oxide glass in 1845[11], is based on the magnetism of a material as mentioned above. Hence, θ increases with magnetic susceptibility, although other parameters also contribute to this phenomenon. Compared with paramagnetic, ferromagnetic, and ferrimagnetic materials, diamagnetic ones exhibit smaller magnetic susceptibilities and hence, smaller θ values. However, the magnetic susceptibility, and hence, θ of diamagnetic materials does not substantially vary with temperature, which is advantageous for practical applications[12].

The magnetic susceptibility of diamagnetic materials is proportional to the number of electrons and mean squared electron–nucleus distance in each constituent ion or atom. Hence, the Faraday effect is larger for glasses with ions of high-atomic-number elements featuring abundant electrons and outermost electrons located far from the nucleus. Indeed, elements with large atomic numbers, such as heavy metals, markedly contribute to large θ values of diamagnetic origin, and oxide glasses with high contents of PbO, Bi_2O_3, and TeO_2 have been extensively investigated[13–22]. In addition to oxide glasses, chalcogenide glasses have been explored to obtain large θ by replacing the oxide ion with anions of large-atomic-number elements such as sulfur and selenium[23–30].

Magnetization is proportional to the strength of a sufficiently weak magnetic field in both diamagnetic and paramagnetic materials. Hence, under these conditions, θ linearly varies with the magnetic field or magnetic flux density. In addition, θ is also proportional to the light path length inside the magnetic material. The Verdet constant (V), defined as

$$V=\frac{\theta}{Bl} \tag{1}$$

is used to estimate the intrinsic strength of the Faraday effect, where B is the strength of the magnetic flux density, and l is the light path length. Table 1 summarizes the Verdet constants of diamagnetic oxide and sulfide glasses, revealing that PbO-, Bi_2O_3-, and TeO_2-based glasses exhibit Verdet constants exceeding those of SiO_2[31] and soda lime silicate glasses[30]. In heavy element–containing oxide glasses, Pb^{2+}, Bi^{3+}, and Te^{4+} ions feature a ground-state outermost electron configuration of $6s^2$, and the electronic transition from $6s^2$ to $6s^16p^1$ contributes to the Verdet constant. Notably, SiO_2 glass exhibits the advantage of very high transmittance even in the ultraviolet region (V = 70.1 rad·T^{-1}·m^{-1} at 193 nm) [32], where heavy-metal-oxide glasses show intense absorption. Table 1 also indicates that sulfide glasses possess large Verdet constants.

The Faraday effect in diamagnetic oxide glasses has been exploited in electric-current transducers based on the sensing of current-generated magnetic fields[14, 17, 18, 33–38] and exhibiting the benefits of reduced noise and wide measurement range. Sensing performance was explored for diamagnetic oxide glasses including TeO_2–ZnO–Na_2O[14, 33], PbO–B_2O_3[18], PbO–Bi_2O_3–GeO_2–B_2O_3[19], TeO_2–PbO–ZnO–BaF_2[34], TeO_2–Bi_2O_3–Li_2O–ZnO[35], flint glass (a type of lead silicate glass) [36], and SiO_2[37] systems. Bulk and fiber forms of these glasses were examined. According to Eq. (1), larger θ values are expected for the fiber form because of its longer light path.

Table 1　Verdet constants of heavy-metal-oxide, sulfide, SiO_2, and soda lime silicate glasses

Glass composition	Verdet constant/ (rad·T^{-1}·m^{-1})	Wavelength/ nm	Reference
$20TeO_2$·80PbO	37.2	700	[13]
$75TeO_2$·20ZnO·$5Na_2O$	28.1	633	[14]
$70TeO_2$·20ZnO·$5Na_2O$·5BaO	25.2	633	[15]
$80TeO_2$·15ZnO·5BaO	32.8	632	[16]
$50.8TeO_2$·29.2PbO·$20B_2O_3$·$10TiO_2$	55.1	633	[17]
80PbO·$20B_2O_3$	51.1	633	[18]
55PbO·$25Bi_2O_3$·$15GeO_2$·$5B_2O_3$	44.2	633	[19]
45PbO·$45Bi_2O_3$·$10SeO_2$	38.7	633	[20]
SiO_2	3.7	633	[31]
Soda lime silicate	5.5	600	[30]
As_2S_3	61	633	[23]
$80GeS_2$·$20Sb_2S_3$	73.6	635	[24]
$75GeS_2$·$25Ga_2S_3$	40.1	635	[25]
$60GeS_2$·$15In_2S_3$·$25PbI_2$	83.2	635	[26]

The approximate composition of soda lime silicate glass is 67.5% (in mass fraction, the same below) SiO_2, 9.0% CaO, 8.5% Na_2O, 8.5% K_2O, and several mass fraction of Al_2O_3, ZnO, TiO_2, and Sb_2O_3 [30].

3 Faraday effect in paramagnetic oxide glasses containing rare-earth ions

This section deals with the Faraday effect in oxide glasses rich in rare-earth ions, which are a prototype of paramagnetic glasses. Early pioneering works on the Faraday effect in paramagnetic oxide glasses have been performed by Berger *et al*.[8] and Rubinstein *et al*.[9] for trivalent rare-earth phosphate and borate glasses, respectively. Verdet constants were measured at different wavelengths for glasses containing trivalent rare-earth ions except La^{3+} and Lu^{3+}, which possess no magnetic moments, as well as Pm^{3+}, which is radioactive. Large Verdet constants were observed for Ce^{3+}, Pr^{3+}, Tb^{3+}, and Dy^{3+}, and small ones for Sm^{3+}, Eu^{3+}, Gd^{3+}, and Tm^{3+}. Shafer *et al.*[10] discovered that $EuO–Al_2O_3–B_2O_3$ glasses containing Eu^{2+} exhibit fairly large Verdet constants despite the small contribution of Eu^{3+} to the Faraday effect demonstrated for the abovementioned phosphate and borate glasses. Thus, the Verdet constant depends on the valence state and type of rare-earth element, which can be attributed to the differences in the magnitude of the magnetic moment of rare-earth ions and spin transition process described below. To date, numerous works have focused on the Faraday effect in fluoride and oxide glasses containing rare-earth ions[39–95].

The Verdet constant of a paramagnetic material, *e.g*., rare earth-containing oxide glass, is related to the spin transition (Fig. 2) as[96]

$$V=\frac{4\pi^2\nu^2\chi}{g\mu_{\mathrm{B}}ch}\sum_j\frac{C_j}{\nu^2-\nu_j^2} \tag{2}$$

where χ is the magnetic susceptibility, ν is the frequency of incident light, g is the Landé g factor, μ_{B} is the Bohr magneton, c is the velocity of light in vacuum, h is the Planck constant, ν_j is the frequency of the j^{th} transition, and C_j is the transition probability of the j^{th} transition, respectively. For the magnetic susceptibility of a paramagnet, the following Curie's law holds:

$$\chi=\frac{N\mu^2}{3k_{\mathrm{B}}T} \tag{3}$$

where μ is the magnetic moment, N is the number of magnetic moments per unit volume, k_{B} is the Boltzmann constant, and T is the absolute temperature. Eq. (2) and Eq. (3) suggest that the magnitude of the Verdet constant ($|V|$) increases with N, *i.e*., with the content of rare-earth ions for oxide glasses rich in rare-earth elements. Thus, since the abovementioned pioneering works on rare-earth phosphate and borate glasses, numerous studies have attempted to maximize the content of rare-earth ions in glasses. Eq. (2) and Eq. (3) also indicate that the contribution of a rare-earth ion to the Verdet constant is positively correlated with its magnetic moment. Hence, the fact that Tb^{3+}, Dy^{3+}, and Eu^{2+} give rise to high $|V|$ can be explained by the large theoretical magnetic moments of these ions (9.7, 10.6 μ_{B}, and 7.9 μ_{B} for the paramagnetic states of Tb^{3+}, Dy^{3+}, and Eu^{2+}, respectively). The theoretical magnetic moment of Eu^{3+} is zero, whereas the experimental one is 3.4 μ_{B} because of Van Vleck paramagnetism. The difference in the magnetic-moment magnitude between Eu^{2+} and Eu^{3+} is one reason of why Eu^{2+} brings about large $|V|$ in oxide glasses whereas Eu^{3+} does not.

A single-oscillator model based on the Van Vleck–Hebb theory [Eq. (2)] is often used to analyze the Faraday effect in oxide glasses rich in rare-earth ions. In other words, only the single process of spin excitation that leads to the Faraday effect is considered. This model provides the following relation:

$$\frac{1}{V}=\frac{g\mu_{\mathrm{B}}ch}{4\pi^2\chi C_{\mathrm{t}}}\left(1-\frac{\lambda^2}{\lambda_{\mathrm{t}}^2}\right) \tag{4}$$

where λ is the wavelength of incident light, λ_{t} is the effective transition wavelength, and C_{t} is the effective transition probability. Eq. (4) indicates that the inverse of the Verdet constant is proportional to the square wavelength of incident light. The validity of this relation has been confirmed for many oxide glasses containing rare-earth ions. Fig. 3 depicts this relation for $15EuO·85[xNa_2O·(1−x)B_2O_3]$ glasses with x = 0.1, 0.2, and 0.3[64], revealing that it holds for all compositions. Based on the horizontal intercept of the corresponding straight-line fits, λ_{t} for x = 0.1, 0.2, and 0.3 equals 386, 403 nm, and 417 nm. As the Faraday effect in rare earth-containing oxide glasses is based on the electronic transition from the 4f ground state to the 5d excited state, λ_{t} corresponds to the energy difference between these states. For $EuO–Na_2O–B_2O_3$ glasses, the inverse of λ_{t}, i.e., the energy difference between 4f (strictly speaking, $^8S_{7/2}$) and 5d states, monotonically decreases with an increase in the optical basicity of the glass defined by

Duffy *et al*. [97–98]. A large optical basicity corresponds to a high electron density on the oxide ions constituting the glass structure, leading to a stronger crystal field around Eu^{2+}. Consequently, the crystal field splitting increases, and the energy difference between the 4f and 5d states, *i.e.*, the inverse of the effective transition wavelength, decreases.

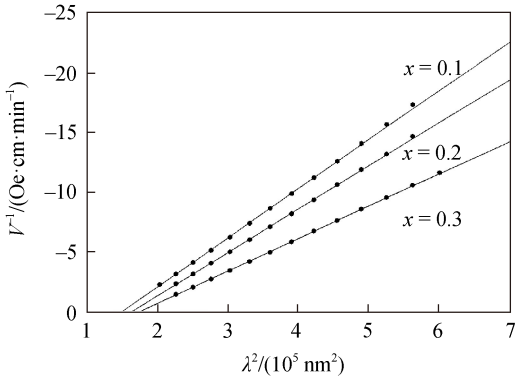

Note: Closed circles represent experimental data, and solid lines represent linear fits based on Eq. (4) [64].

Fig. 3　Relation between the inverse of the Verdet constant and square of incident-light wavelength for 15EuO·85 [xNa$_2$O·(1 − x)B$_2$O$_3$] glasses

Eq. (4) suggests that $|V|$ increases with an increase in C_t and λ_t at a fixed wavelength. As described above, Ce^{3+} and Pr^{3+} can lead to large $|V|$ despite having smaller magnetic moments than Dy^{3+} and Tb^{3+}. The large $|V|$ values of oxide glasses containing Ce^{3+} and Pr^{3+} are ascribable to the large C_t values of these ions. For Eu^{2+}, not only the large magnetic moment but also the long effective wavelength (λ_t) can contribute to the increased $|V|$.

Whereas Eu^{2+} causes a large Faraday effect, Gd^{3+} does not, although these ions have the same ground-state electronic configuration ($4f^7$) and hence, magnetic moment (7.9 μ_B). This behavior is attributable to the energy difference between the 4f and 5d states, which is much larger for Gd^{3+}. Hence, λ_t for Gd^{3+} is shorter than that for Eu^{2+}, and the former ion cannot provide a large $|V|$, especially in the visible range.

As described above, glasses with higher contents of rare-earth ions should exhibit larger $|V|$ values. However, rare earths typically induce crystallization when present in oxide glasses at high levels. This problem can be overcome using containerless processing[99–100], which has been proven effective for expanding the glass-forming region of many systems and creating glasses with novel compositions unattainable by conventional melt quenching. For instance, containerless processing has been used to fabricate La_2O_3–Ga_2O_3 glasses with a wide composition range[101]. These glasses are transparent in a broad wavelength range (ultraviolet to mid-infrared), show low phonon energy, and can include large amounts of Er^{3+} and exhibit intense photoluminescence without concentration quenching even at high Er^{3+} contents[102]. Containerless processing has been applied to oxide glasses showing the Faraday effect, *e.g.*, Suzuki *et al*[69]. prepared Tb_2O_3–Al_2O_3–B_2O_3–SiO_2 glasses, achieving Tb_2O_3 contents exceeding those achievable through conventional melt quenching. Fig. 4 presents the wavelength dependences of the Verdet constants of Tb_2O_3–Al_2O_3–B_2O_3–SiO_2 glasses and single-crystalline TGG, revealing that all glasses exhibit $|V|$ values exceeding that of TGG over the whole wavelength range. The largest $|V|$ is observed for the glass denoted as 60T, which contains 60% (in mole fraction) Tb_2O_3 and has been commercialized as an optical isolator for Nd^{3+}:$Y_3Al_5O_{12}$ (Nd:YAG) lasers by Nippon Electric Glass Co., Ltd. Sasaki *et al*.[71] used containerless processing to prepare Tb_2O_3–Dy_2O_3–B_2O_3 glasses with $|V|$ values exceeding that of single-crystalline TGG. Xie *et al*.[61] prepared B_2O_3–Ga_2O_3 (Al_2O_3) glasses containing Tb_2O_3 and Ce_2O_3 *via* containerless processing, revealing that their $|V|$ values (98.8–202.6 rad·T^{-1}·m^{-1} at 633 nm) exceeded that of TGG.

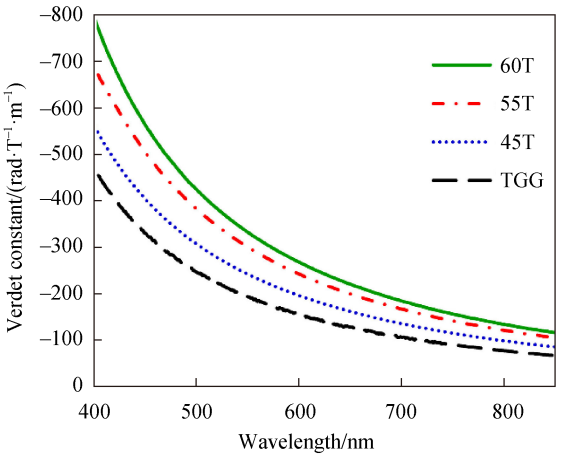

Fig. 4　Wavelength dependence of the Verdet constant for Tb_2O_3–Al_2O_3–B_2O_3–SiO_2 glasses prepared *via* containerless processing and single-crystalline TGG ($Tb_3Ga_5O_{12}$) [69]

The Verdet constants of several rare earth–rich oxide glasses are listed in Table 2. During these five years, most studies on the Faraday effect in paramagnetic glasses have focused on Tb_2O_3-based glasses. Table 2 indicates that $|V|$ monotonically increases with the increasing Tb^{3+} content of Tb_2O_3-rich glasses. Optical absorption spectra and magneto-optical figures of merit were reported for some Tb_2O_3-rich glasses[61, 69, 72–74]. For Tb_2O_3–Al_2O_3–B_2O_3–GeO_2–P_2O_5 glasses, the figure of merit increases with increasing/decreasing wavelength, peaking at 420–450 nm depending on the Tb_2O_3 content, in a wavelength range between 400 nm and 800 nm[72]. The tendency that the figure of merit increases in the visible but decreases in a shorter wavelength region as the wavelength decreases was also observed for Tb_2O_3–Ga_2O_3–B_2O_3 glasses[73]. The reduced figure of merit in the shorter-wavelength region is ascribable to the interband transition of the glass. An Al_2O_3–B_2O_3–SiO_2 glass with 60% (in mole fraction) Tb_2O_3 exhibits a large figure of merit exceeding that of single-crystalline TGG in the visible range[69].

Table 2 Verdet constants of rare earth–rich glasses

Glass composition	Verdet constant/ (rad·T^{-1}·m^{-1})	Wavelength/ nm	Reference
$27.2Ce_2O_3·72.8P_2O_5$	–50.3	635	[8]
$25.4Tb_2O_3·74.6P_2O_5$	–55.3	635	[8]
$28.5Dy_2O_3·71.5P_2O_5$	–57.3	635	[8]
$14.6Tb_2O_3·12.4Pr_2O_3·73.0B_2O_3$	–89	635	[9]
$15.4Dy_2O_3·13.1Pr_2O_3·71.5B_2O_3$	–84.4	635	[9]
$35Tb_2O_3·15Al_2O_3·30B_2O_3·15GeO_2·5P_2O_5$	–140.15	632.8	[72]
$40Tb_2O_3·3Li_2O·2MgO·15B_2O_3·40GeO_2$	–143.04	633	[76]
$45Tb_2O_3·5Ga_2O_3·35B_2O_3·15GeO_2$	–105	650	[78]
$45Tb_2O_3·3ZnO·15B_2O_3·32GeO_2·5P_2O_5$	–168.55	633	[79]
60T glass (Al_2O_3-B_2O_3-SiO_2 with 60 mol% Tb_2O_3)	–234	633	[69]
$58Tb_2O_3·42B_2O_3$	–229	633	[71]
$30Tb_2O_3·40TbF_3·30(SiO_2$-$B_2O_3)$	–146.91	638	[75]
$40Tb_2O_3·10Dy_2O_3·16.7B_2O_3·10Ga_2O_3·10SiO_2·3.3P_2O_5$	–185.3	632.8	[50]
$30Tb_4O_7·8Dy_2O_3·11PbO·25B_2O_3·12SiO_2·14GeO_2·0.5Sb_2O_3$	–162.9	633	[77]
$45Tb_2O_3·1Pr_6O_{11}·32GeO_2·15B_2O_3·3ZnO·5P_2O_5$	–175.22	633	[74]
$53Tb_2O_3·0.5Ce_2O_3·7Ga_2O_3·39.5.B_2O_3$	–202.6	633	[61]
$40Tb_2O_3·10Ho_2O_3·3ZnO·20B_2O_3·32GeO_2·5P_2O_5$	–172.65	633	[60]
$34.2EuO·14.8Al_2O_3·50.7B_2O_3$	–139	600	[10]
$30EuO·70B_2O_3$	–106	600	[64]
$58EuO·12Al_2O_3·20B_2O_3·10SiO_2$	–300	633	[68]

From the viewpoint of practical applications, not only $|V|$ and the magneto-optical figure of merit but also other factors including thermal stability and chemical durability are crucial. The thermal stability of glass is commonly discussed in terms of its glass transition temperature (T_g) and difference (ΔT) between T_g and the crystallization temperature. For example, T_g and ΔT were reported to be 600–650 °C and approximately 140 °C, respectively, for Tb_2O_3–TbF_3–SiO_2–B_2O_3 glasses[75], representing sufficient thermal stability. Tb_2O_3-rich glasses tend to show an increase in T_g and a decrease in ΔT with increasing Tb_2O_3 content[61, 69]. Nonetheless, the relatively high T_g of these glasses ensures good thermal stability. Chemical durability was examined for Tb_2O_3–GeO_2–B_2O_3–ZnO–P_2O_5 glasses doped with rare-earth ions[74]. These glasses were found to be highly resistant to water and basic aqueous solutions but readily dissolved in aqueous HCl. The poor acid resistance of Tb_2O_3-rich glasses was ascribed to the similarity between the chemical properties of rare-earth oxides and alkali-metal and alkaline-earth-metal oxides. Furthermore, Tb_2O_3–GeO_2–B_2O_3–ZnO–P_2O_5 glasses were found to provide protection from γ-rays[81].

Rare-earth oxide–based paramagnetic glasses as well as the abovementioned diamagnetic glasses find applications in magnetic-field sensing[55, 83], current sensing[75, 82], and optical isolation[103]. Moreover, Tb_2O_3–Li_2O–CaO–B_2O_3 glasses can be used to fabricate waveguides[84].

4 Faraday effect in Eu^{2+}-containing ferromagnetic amorphous oxides

The fundamental magnetism of transition metal-rich ionic glasses, including oxide and fluoride ones, is interesting from at least two aspects. First, these glasses can be classified as random-spin systems with strongly frustrated magnetic moments, as exemplified by the so-called spin glasses[104–105]. Spin glasses have been extensively characterized from the experimental and theoretical points of view, and some physicists who greatly contributed to the progress in theoretical

interpretation of spin glass and application of the theory to other fields received Nobel prize in physics[106]. Second, considering the abundance of ferromagnetic amorphous alloys, a question arises whether it is possible or not to obtain ionic glasses that undergo ferromagnetic phase transition. The ferromagnetism observed in amorphous alloys is essentially the same as that in crystalline metals and alloys; both amorphous and crystalline alloys possess Curie temperatures at which they exhibit second-order phase transitions between ferromagnetic and paramagnetic states.

The interest in random-spin systems has triggered research on the magnetic properties of oxide and fluoride glasses rich in transition-metal ions. Verhelst *et al*.[107] measured the alternating-current (AC) magnetic susceptibilities of $CoO–Al_2O_3–SiO_2$ and $MnO–Al_2O_3–SiO_2$ glasses at varied temperatures and found that the susceptibility–temperature plots exhibited cusp-like sharp peaks at certain temperatures. For $CoO–Al_2O_3–SiO_2$ glasses, Rechenberg *et al*.[108] observed the long-time relaxation behavior of remanent magnetization. Sanchez *et al*.[109] explored the temperature dependence of AC magnetic susceptibility for $FeO–Al_2O_3–SiO_2$ glasses at varied frequencies of AC magnetic fields and found that the spin-freezing temperature (T_f), at which susceptibility is maximized, increases with frequency. The frequency dependence of T_f was analyzed using the Vogel–Fulcher law. Shaw *et al*.[110] obtained zero-field-cooled (ZFC) and field-cooled (FC) magnetic susceptibilities as functions of temperature for $Fe_2O_3–P_2O_5$ glasses. The ZFC susceptibility exhibited a cusp-like peak at T_f and decreased with decreasing temperature below T_f, whereas the FC susceptibility was almost independent of temperature below T_f. Both ZFC and FC susceptibilities showed the same temperature dependence above T_f. Renard *et al*.[111] measured the temperature dependence of AC magnetic susceptibility for $PbMnFeF_7$ and Pb_2MnFeF_9 fluoride glasses, revealing that the cusp-like peak at T_f became rounded when a direct-current (DC) magnetic field was applied simultaneously with the AC magnetic field.

Akamatsu *et al*.[112–116] examined the magnetic properties of iron oxide–based glasses, including $Fe_2O_3–TeO_2$, $Fe_2O_3–Bi_2O_3–B_2O_3$, $FeO–Fe_2O_3–P_2O_5$, and $Fe_2O_3–R_2O_3$ (R = Sm, Gd, and Tb)–$Al_2O_3–B_2O_3$ systems, focusing on the effect of aging in a magnetic field for $20Fe_2O_3·80TeO_2$. This glass was cooled to 3 K at 0.2 K·min^{-1} in the absence of a magnetic field. Then, a DC magnetic field of 5 Oe was applied, and susceptibility was measured upon warming at 0.2 K min^{-1} until a stopping temperature (T_s) was reached. At T_s, the sample was kept for 5.5 h, and the time dependence of magnetic susceptibility was measured. Subsequently, the sample was warmed at 0.2 K·min^{-1}, and susceptibility was obtained. The results of these measurements are shown in Fig. 5[112]. In this case, T_s equaled 4 K and 5 K. Magnetic susceptibility increased with time at each T_s during aging (Fig. 5, inset), decreasing with an increase in temperature after aging. Eventually, susceptibility merged with the reference curve obtained for the ZFC process without aging at any temperature. This phenomenon was attributed to the rejuvenation effect. The inset of Fig. 5 indicates that magnetic susceptibility logarithmically scaled with time during aging in a magnetic field.

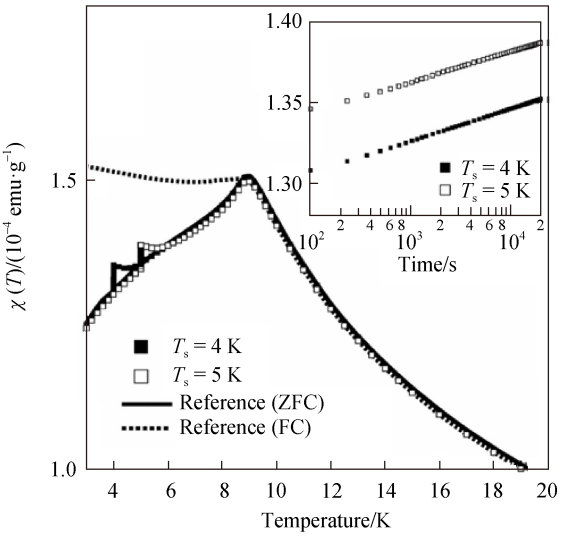

Note: For the ZFC process, aging in a magnetic field was performed at T_s = 4 and 5 K for 5.5 h. The rejuvenation effect was observed. Inset represents the time dependence of magnetic susceptibility at 4 K and 5 K.

Fig. 5　Zero-field-cooled (ZFC) and field-cooled (FC) magnetic susceptibility as a function of temperature for $20Fe_2O_3·80TeO_2$ glass [112].

The abovementioned phenomena observed for oxide and fluoride glasses containing transition elements reveal that these glasses experience spin glass transitions at low temperatures. The temperature dependence of magnetic susceptibility of these ionic glasses at temperatures

sufficiently exceeding T_f obeys the following Curie–Weiss law instead of Eq. (3):

$$\chi = \frac{N\mu^2}{3k_B(T - T_w)} \tag{5}$$

Here, T_w is the Weiss temperature and takes a negative value for all ionic glasses described above, which indicates the dominance of the antiferromagnetic interaction. The combination of (1) magnetic frustration arising from the antiferromagnetic coupling among the nearest-neighbor magnetic moments and (2) the random distribution of magnetic moments due to the random glass structure inevitably leads to a spin glass phase.

In contrast, a positive T_w was found for an amorphous silicate with a composition of $Eu^{2+}_{0.12}Eu^{3+}_{0.02}Si_{0.31}O_{0.55}$[117], suggesting that the interaction among the Eu ions in this material is ferromagnetic. However, T_w was as low as 1 K, and the ferromagnetic transition did not occur above at least 1.5 K. Conversely, the $60.0EuO{\cdot}11.0Al_2O_3{\cdot}19.5B_2O_3{\cdot}9.5SiO_2$ glass exhibited a clear ferromagnetic–paramagnetic transition at 2.2 K[118]. EuO–Al_2O_3–B_2O_3–SiO_2 glasses also show large Faraday effects at room temperature.

Fig. 6a illustrates the wavelength dependence of the Verdet constant for EuO–Al_2O_3–B_2O_3–SiO_2 and other glasses [$46.7EuO{\cdot}13.3Al_2O_3{\cdot}13.3B_2O_3{\cdot}26.7SiO_2$ (47EABS), $58.0EuO{\cdot}12.0Al_2O_3{\cdot}20.0B_2O_3{\cdot}10.0SiO_2$ (58EABS), $30EuO{\cdot}15Na_2O{\cdot}55SiO_2$ (+)[66], $30Tb_2O_3{\cdot}70B_2O_3$ (×)[62], and $40Tb_2O_3{\cdot}10Dy_2O_3{\cdot}16.7B_2O_3{\cdot}10Ga_2O_3{\cdot}10SiO_2{\cdot}3.3P_2O_5$ (*)[50]][68]. The $|V|$ of 58EABS (378 $rad{\cdot}T^{-1}{\cdot}m^{-1}$) exceeds that of the containerless processing-derived 60T glass shown in Fig. 4. Fig. 6b indicates that the inverse of the Verdet constant is proportional to the square of the wavelength of incident light, confirming that Eq. (4) is a good approximation.

The ferromagnetic transition was also demonstrated for amorphous EuO–TiO_2 thin films prepared by pulsed laser deposition[119]. Fig. 7 depicts the temperature dependence of magnetization for amorphous $EuTiO_3$ (a-ETO) and Eu_2TiO_4 (a-2ETO) thin films, revealing a drastic increase at a certain temperature upon cooling, which suggests a paramagnetic-to-ferromagnetic phase transition. The transition temperature, *i.e.*, Curie temperature estimated from the inflection point of the magnetization–temperature curve (arrows in Fig. 7) is 5.5 K and 14.0 K for amorphous $EuTiO_3$ and Eu_2TiO_4, respectively. A comparison

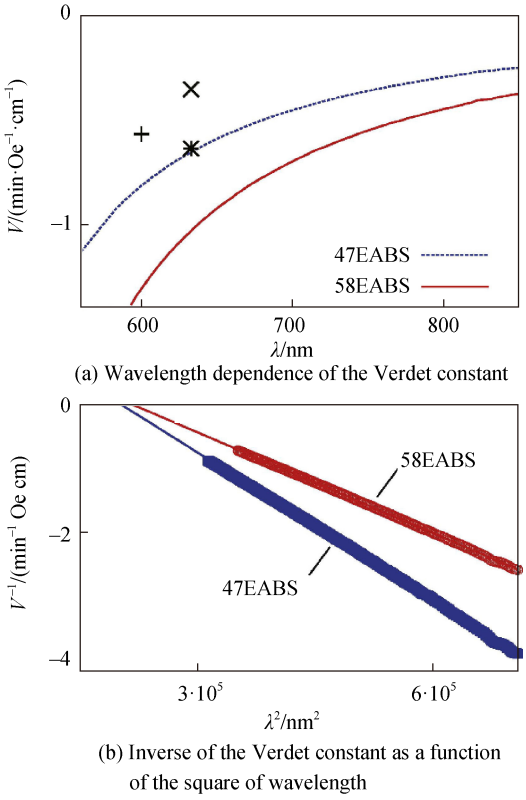

(a) Wavelength dependence of the Verdet constant

(b) Inverse of the Verdet constant as a function of the square of wavelength

Fig. 6 Faraday effect in EuO- and Tb_2O_3-based glasses [68]

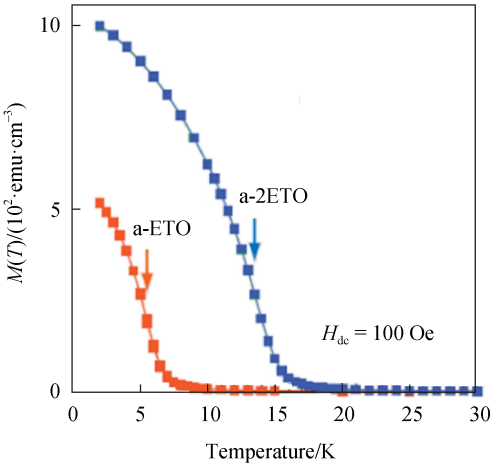

Fig. 7 Relationship between magnetization and temperature for amorphous $EuTiO_3$ (a-ETO) and Eu_2TiO_4 (a-2ETO) thin films, revealing the occurrence of a ferromagnetic transition in both cases. Arrows represent the Curie temperature [119]

of these values with those of the corresponding crystalline counterparts reveals interesting results. Crystalline $EuTiO_3$ and Eu_2TiO_4 are an antiferromagnet with a Néel temperature of 5.3 K[120] and a ferromagnet with a Curie temperature of 9 K[121], respectively. First,

amorphous $EuTiO_3$ is ferromagnetic, although its crystalline counterpart is antiferromagnetic. The magnetic transition temperatures of these two phases are almost identical. Second, both crystalline and amorphous phases of Eu_2TiO_4 are ferromagnetic, although the Curie temperature is higher for the amorphous phase. These are very rare phenomena, as the magnetic transition temperature of amorphous oxides is usually much lower than that of their crystalline counterparts. For instance, crystalline YIG, which exhibits a large Faraday effect and is commercially available as an optical isolator for optical telecommunications, is ferrimagnetic and has a Curie temperature of 560 K[122], whereas the magnetic phase transition temperature of its amorphous state is only 40 K[123]. Moreover, although crystalline $BiFeO_3$ is antiferromagnetic below 643 K[124], its amorphous counterpart exhibits a spin glass transition at 20 K[125].

The ferromagnetism of amorphous $EuTiO_3$ and Eu_2TiO_4 is ascribable to the local structure or coordination environment of Eu^{2+}. The mechanism of ferromagnetism observed for oxides containing Eu^{2+} ions is schematically illustrated in Fig. 8[121]. A 4f spin in one Eu^{2+} can be excited to the 5d level and then transferred to the 5d level of the nearest-neighboring Eu^{2+} with a certain probability. The transferred spin interacts with existing 4f spins in the nearest-neighboring Eu^{2+} so that all spin magnetic quantum numbers of 4f and 5d electrons are the same according to Hund's rule. Consequently, the magnetic moments of nearest-neighboring Eu^{2+} become parallel to each other.

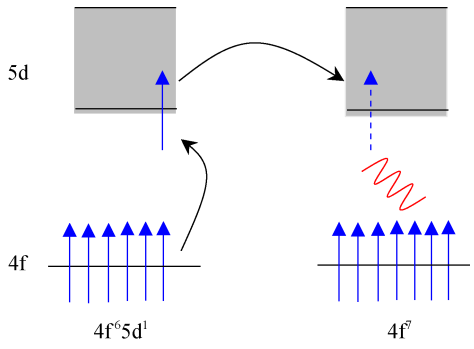

Fig. 8　Schematic mechanism leading to a ferromagnetic interaction between nearest-neighboring Eu^{2+} ions in oxides

This ferromagnetic interaction competes with antiferromagnetic coupling between Eu^{2+} ions arising from superexchange interaction. The outcome of the competition between ferromagnetic and antiferromagnetic interactions depends on the crystal field strength around Eu^{2+}. A stronger crystal field enlarges the splitting of the 5d levels, decreasing the energy difference between the 4f and lowest 5d levels. In this case, the excitation of the 4f spin to the lowest 5d level is facilitated, and the ferromagnetic interaction between Eu^{2+} becomes preferred. The crystal field strength is expected to increase with the decreasing oxygen coordination number (CN) of Eu^{2+} because smaller CNs give rise to shorter Eu^{2+}—O^{2-} bonds. Extended X-ray absorption fine structure spectroscopy analysis revealed that the CN of Eu^{2+} in amorphous $EuTiO_3$ and Eu_2TiO_4 is 6[126], whereas those in crystalline $EuTiO_3$ and Eu_2TiO_4 are 12 and 9, respectively. Therefore, whereas the antiferromagnetic interaction between Eu^{2+} ions is dominant in crystalline $EuTiO_3$, the ferromagnetic interaction is dominant in amorphous $EuTiO_3$.

Amorphous $EuTiO_3$ and Eu_2TiO_4 thin films exhibit large Faraday effects because of their ferromagnetic properties despite having lower-than-ambient Curie temperatures. Fig. 9 presents the Verdet constant as a function of incident light wavelength for these amorphous oxides[127]. The largest $|V|$ is higher than 5000 $rad \cdot T^{-1} \cdot m^{-1}$, exceeding that of the abovementioned 58EABS glass by one order of magnitude. The $|V|$ and its wavelength dependence of amorphous $EuTiO_3$ and Eu_2TiO_4 are very similar to those of crystalline EuSe[128],

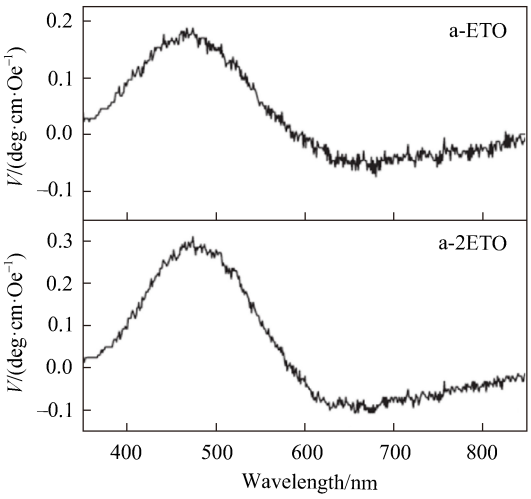

Fig. 9　Wavelength dependence of Verdet constant for amorphous $EuTiO_3$ (a-ETO) and Eu_2TiO_4 (a-2ETO) thin films at room temperature [127]

which is a magnetic semiconductor. The behavior of Verdet constant in Fig. 9, *i.e.*, wavelength-dependent sign reversal, was also observed for EuO[5], (Cd,Mn)Te[6], and EuSe[128]. The wavelength at which the sign of the Verdet constant changes corresponds to the electronic transition from $4f^7$ to $4f^65d$ in EuSe. The absorption spectra of amorphous $EuTiO_3$ and Eu_2TiO_4 feature a broad absorption band centered at ~410 nm[127]. Therefore, the above sign change observed for amorphous EuO–TiO_2 is thought to have the same origin as that observed for EuSe.

5 Faraday effect in paramagnetic oxide glasses containing 3d transition-metal ions

Compared with that observed for oxide glasses containing rare-earth elements, the Faraday effect observed for oxide glasses containing 3d transition metals is underexplored, possibly because the strong antiferromagnetic interactions among transition-metal ions in oxide glasses (see Section 4) reduce magnetic susceptibility at room temperature. Another reason may be the intense optical absorption in the visible range due to transition-metal ions, which decreases the magneto-optical figure of merit and thus hinders practical applications. Thus far, the Faraday effect has been reported for oxide glasses containing Mn^{2+}[129–133], Fe^{2+}[134], and Ni^{2+}[135]. Fig. 10 depicts the optical absorption spectra and photographs of xFeO·(100 − x)P_2O_5 glasses with x = 50.0, 54.0, and 57.1[134]. Notably, these glasses are rather transparent to visible light, whereas a high content of Fe^{3+} ions renders oxide glasses dark because of intense absorption in the visible range. As intense absorption is observed at above 700 nm and below 400 nm, the single-oscillator model is not appropriate for analyzing the wavelength dependence of the Verdet constant of FeO–P_2O_5 glasses. Hence, the following equation is used instead of Eq. (4)[134]:

$$V=\frac{4\pi^2\chi}{g\mu_B ch}\left[C_1\left(1-\frac{\lambda^2}{\lambda_1^2}\right)^{-1}+C_2\left(1-\frac{\lambda^2}{\lambda_2^2}\right)^{-1}\right] \quad (6)$$

For instance, the 57.1FeO·42.9P_2O_5 glass features $C_1 = 8.6 \times 10^{-45}$ J·cm^3, λ_1 = 214 nm, $C_2 = 1.1 \times 10^{-46}$ J·cm^3, and λ_2 = 1100 nm. These values correspond to the intensities and wavelengths of two optical absorption bands appearing in Fig. 10. The $|V|$ of the 57.1FeO·42.9P_2O_5 glass at 405 nm (59 rad·T^{-1}·m^{-1}) is smaller than those of EuO- and Tb_2O_3-based glasses described above. However, the FeO–P_2O_5 glass is composed of earth-abundant elements, *i.e.*, O, Fe, and P.

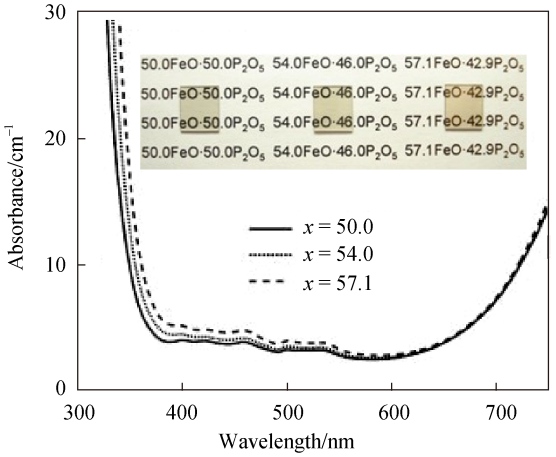

Fig. 10 Optical absorption spectra and photographs of xFeO·(100 − x)P_2O_5 glasses [134]

6 Faraday effect in glass-ceramics composed of magnetic nanocrystals and a glass matrix

The Faraday effect in glass-ceramics comprising magnetic nanocrystals in a glass matrix has also been investigated. Combinations of oxide glass matrices with not only ferro- and ferrimagnetic nanocrystals but also paramagnetic and even diamagnetic nanocrystals have been reported (Table 3) [136–152]. As ferro- and ferrimagnetic materials such as Fe, Co, Ni and their alloys as well as ferrites, *i.e.*, iron oxide-based compounds, exhibit large magnetization even at room temperature, glass-ceramics containing nanocrystals of these materials are expected to show large Faraday effects. Indeed, the Verdet constant of amorphous FeO–SiO_2 thin films with dispersed Fe nanoparticles reaches 4.22×10^4 rad·T^{-1}·m^{-1} at 400 nm[136], exceeding those of typical paramagnetic glasses rich in rare-earth ions by two orders of magnitude (see Table 2).

In general, an increase in the size of magnetic crystalline particles and volume fraction of the crystalline phase leads to an increase in the magnetization per unit volume and hence, the θ of glass-ceramics. However, this increase also intensifies the absorption and scattering of incident light, thus increasing optical loss. Light scattering

Table 3　Glass-ceramics composed of a magnetic nanocrystalline phase and an oxide glass matrix for which the Faraday effect was examined

Crystalline phase	Magnetism of crystalline phase	Glass matrix	Reference
Fe	Ferromagnetic	FeO-SiO_2	[136]
Au-Ni	Ferromagnetic	PbO-B_2O_3-TeO_2	[137]
Fe_3O_4	Ferrimagnetic	Na_2O-CaO-SiO_2	[138–139]
Fe_3O_4	Ferrimagnetic	SiO_2 (gel)	[140]
$NiFe_2O_4$	Ferrimagnetic	ZnO-Al_2O_3-P_2O_5-TeO_2	[141]
$La_{0.8}Sr_{0.2}FeO_3$	Weak ferromagnetic	PbO-Bi_2O_3-Al_2O_3-B_2O_3	[142]
$MnSe_2$:Eu	Ferromagnetic	PbO-Bi_2O_3-B_2O_3	[143]
$Gd_3Al_2Ga_3O_{12}$	Paramagnetic	PbO-B_2O_3-TeO_2	[144]
$Y_3Al_5O_{12}$:Tb^{3+}	Paramagnetic	SiO_2	[145]
TbOF:Pr^{3+}	Paramagnetic	$NaPO_3$-BaF_2	[146]
$TbVO_4$:Y^{3+}	Paramagnetic	PbO-Bi_2O_3-B_2O_3-GeO_2	[147]
YbF_3:Pr^{3+}	Paramagnetic	PbO-Bi_2O_3-B_2O_3	[148]
$NaYF_4$: Fe^{3+},Ho^{3+}	Paramagnetic	PbO-Bi_2O_3-B_2O_3-SiO_2	[149]
$AlPO_4$	Diamagnetic	Tb_2O_3-Al_2O_3-B_2O_3-GeO_2-P_2O_5	[150]
Ta_2O_3	Diamagnetic	PbO-Bi_2O_3-B_2O_3	[151]
Sc_2O_3, Lu_2O_3	Diamagnetic	PbO-Bi_2O_3-B_2O_3	[152]

is affected by the difference between the refractive indices of magnetic crystalline particles and the glass matrix as well as by the size of the crystalline-phase particles. Hence, synthesis conditions should be optimized by considering the glass composition and magnetic crystalline phase along with the size, volume fraction, and refractive index of the latter to obtain glass-ceramics with large magneto-optical figures of merit.

The localized surface plasmon resonance (LSPR) of metallic nanoparticles can be used to increase θ[137–139]. Nakashima *et al*.[138–139] prepared Na_2O–CaO–SiO_2 glass in which Fe_3O_4 and Au nanoparticles were precipitated by femtosecond laser irradiation and subsequent thermal annealing, revealing that θ increased at the wavelength corresponding to the LSPR of Au nanoparticles. As optical absorption due to the LSPR takes place in this case, an enhancement of Faraday rotation should overcome this optical loss for practical applications. An alternative way to reduce optical loss is utilizing the Mie resonance observed for dielectric nanoparticles instead of the LSPR of metallic nanoparticles. In this case, dielectrics (materials showing positive and negative dielectric constants are herein defined as dielectrics and metals, respectively) with high refractive indices and low extinction coefficients (*e.g*., TiO_2, ZrO_2, and SiC) are promising candidates. Notably, the Mie resonance of these compounds is very effective in enhancing optical functionality, such as the fluorescence of phosphors[153–155].

7　Summary

The Faraday effect was discovered 180 years ago, and studies on this effect in paramagnetic oxide glasses based on rare-earth elements have been carried out starting from the 1960s. Still, extensive research is being conducted to develop oxide glasses with novel compositions exhibiting large Faraday effects and use them in devices such as optical isolators, electric-current transducers, and magnetic-field sensors. One of the recent topics relevant to the Faraday effect in oxide glasses is the progress in processing enabling the realization of high contents of rare-earth ions in glasses. The large Faraday effect in ferromagnetic amorphous EuO-based oxides, which is comparable with that in crystalline magnetic semiconductors such as EuSe, is another interesting topic, as well as the Faraday effect in glass-ceramics where magnetic nanocrystals are embedded in an oxide glass matrix. Thus, new oxide glass systems exhibiting even larger Faraday effects are expected to be developed in the near future.

Acknowledgement

The author would like to thank Prof. Naohiro Soga (professor emeritus of Kyoto University), Prof. Kazuyuki Hirao (professor emeritus of Kyoto University), Prof. Koji Fujita (Kyoto University), Dr. Shunsuke Murai (Kyoto University; currently, Osaka Metropolitan University), Dr. Hirofumi Akamatsu (Kyoto University; currently, Kyushu University), and all the members who contributed to the present research on Faraday effect of oxide glasses at Kyoto University for their support and collaboration. The author is also deeply grateful to Prof. Jianrong Qiu (Zhejiang University), Prof. Atsunobu Masuno (Kyoto University), Dr. Shunta Sasaki (Kyoto University; currently, Tohoku University), Dr. Futoshi Suzuki (Nippon Electric Glass Co., Ltd.), Dr. Fumio Sato

(Nippon Electric Glass Co., Ltd.), and Dr. Hiroyuki Oshita (Nippon Electric Glass Co., Ltd.) for their fruitful discussions. A part of the present work was financially supported by Nippon Electric Glass Co., Ltd.

References:

[1] SATO K. Hikari-to-Jiki[M]. Tokyo: Asakura Publishing Co., Ltd., 2001.

[2] TAKEUCHI H. The faraday effect of bismuth substituted rare-earth iron garnet[J]. Jpn J Appl Phys, 1975, 14(12): 1903–1910.

[3] SCOTT G B, LACKLISON D E, RALPH H I, et al. Magnetic circular dichroism and Faraday rotation spectra of $Y_3Fe_5O_{12}$[J]. Phys Rev B. 1975, 12(7): 2562–2571.

[4] SUITS J. A review of some recent work in magnetooptical recording[J]. IEEE Trans Magn, 1972, 8(3): 421–425.

[5] MITANI T, ISHIBASHI M, KODA T. Magneto-optical properties of eus film[J]. J Phys Soc Jpn, 1975, 38(3): 731–738.

[6] KOYANAGI T, MATSUBARA K, TAKAOKA H, et al. Epitaxial growth of $Cd_{1-x}Mn_xTe$ films by ionized-cluster beams and their magneto-optical properties[J]. J Appl Phys, 1987, 61(8): 3020–3024.

[7] LEVITIN R Z, ZVEZDIN A K, VON ORTENBERG M, et al. Faraday effect in $Tb_3Ga_5O_{12}$ in a rapidly increasing ultrastrong magnetic field[J]. Phys Solid State, 2002, 44(11): 2107–2111.

[8] BERGER S B, RUBINSTEIN C B, KURKJIAN C R, et al. Faraday rotation of rare-earth (III) phosphate glasses[J]. Phys Rev, 1964, 133(3A): A723–A727.

[9] RUBINSTEIN C B, BERGER S B, VAN UITERT L G, et al. Faraday rotation of rare-earth (III) borate glasses[J]. J Appl Phys, 1964, 35(8): 2338–2340.

[10] SHAFER M W, SUITS J C. Preparation and faraday rotation of divalent europium glasses[J]. J Am Ceram Soc, 1966, 49(5): 261–264.

[11] KNUDSEN O. The Faraday effect and physical theory, 1845–1873[J]. Arch Hist Exact Sci, 1976, 15(3): 235–281.

[12] WILLIAMS P A, ROSE A H, DAY G W, et al. Temperature dependence of the Verdet constant in several diamagnetic glasses[J]. Appl Opt, 1991, 30(10): 1176–1178.

[13] BORRELLI N F. Faraday rotation in glasses[J]. J Chem Phys, 1964, 41(11): 3289–3293.

[14] CHEN Q L, MA Q H, WANG H, et al. Diamagnetic tellurite glass and fiber based magneto-optical current transducer[J]. Appl Opt, 2015, 54(29): 8664–8669.

[15] CHEN Q L, WANG H, WANG Q W, et al. Faraday rotation influence factors in tellurite-based glass and fibers[J]. Appl Phys A, 2015, 120(3): 1001–1010.

[16] HRABOVSKY J, STRIZIK L, DESEVEDAVY F, et al. Optical, magneto-optical properties and fiber-drawing ability of tellurite glasses in the TeO_2–ZnO–BaO ternary system[J]. J Non Cryst Solids, 2024, 624: 122712.

[17] CHEN Q L, ZHANG M, WANG H, et al. Structures and magneto optical property of diamagnetic TiO_2-TeO_2-PbO-B_2O_3 glass[J]. J Non Cryst Solids, 2017, 468: 58–66.

[18] QIAN P Y, WANG S B, WANG Y J. Magneto-optical properties and temperature dependence of diamagnetic lead borate glasses for fiber-optical current transducer[J]. Opt Mater, 2019, 89: 349–354.

[19] CHEN Q L, MA Q H, WANG H, et al. Structural and properties of heavy metal oxide Faraday glass for optical current transducer[J]. J Non Cryst Solids, 2015, 429: 13–19.

[20] CHEN Q L, SU K, LI Y T, et al. Structure, spectra and thermal, mechanical, Faraday rotation properties of novel diamagnetic SeO_2-PbO-Bi_2O_3-B_2O_3 glasses[J]. Opt Mater, 2018, 80: 216–224.

[21] LINGANNA K, JU S, RYU Y, et al. Effect of WO_3 on physical and magneto-optical properties of TeO_2–La_2O_3–WO_3 glasses for magneto-optics application[J]. Results Phys, 2022, 43: 106069.

[22] BARCZAK K, CIMEK J, STĘPIEŃ R, et al. Measurements of Verdet constant in heavy metal oxide glasses for magneto-optic fiber current sensors[J]. Opt Mater, 2022, 123: 111942.

[23] RUAN Y L, JARVIS R A, RODE A V, et al. Wavelength dispersion of Verdet constants in chalcogenide glasses for magneto-optical waveguide devices[J]. Opt Commun, 2005, 252(1–3): 39–45.

[24] CHEN G, XU Y T, GUO H T, et al. Magneto-optical effects of Ge-Ga-Sb(In)-S chalcogenide glasses with diamagnetic responses[J]. J Am Ceram Soc, 2017, 100(7): 2914–2920.

[25] XU Y T, XIAO X S, CUI X X, et al. Improvement of the Faraday effect in Ge-S based chalcogenide glasses *via* gallium and lead compositional modifications[J]. Opt Mater Express, 2018, 8(7): 1754.

[26] XU Y T, GUO H T, XIAO X S, et al. High Verdet constants and diamagnetic responses of GeS_2-In_2S_3-PbI_2 chalcogenide glasses for integrated optics applications[J]. Opt Express, 2017, 25(17): 20410–20420.

[27] QIU J R, KANBARA H, NASU H, et al. Wavelength dispersions of the faraday effect in chalcogenide glasses[J]. J Ceram Soc Japan, 1998, 106(1230): 228–230.

[28] QIU J R, HIRAO K. The Faraday effect in diamagnetic glasses[J]. J Mater Res, 1998, 13(5): 1358–1362.

[29] SNETKOV I L, BLAGIN R D, SHIRYAEV V S, et al. Magneto-optical and thermo-optical properties of the Ge-Sb-As-S glass[J]. Opt Mater, 2023, 143: 114277.

[30] ROBINSON C C. The faraday rotation of diamagnetic glasses from 0334 μ to 19 μ[J]. Appl Opt, 1964, 3(10): 1163.

[31] GARN W B, CAIRD R S, FOWLER C M, et al. Measurement of faraday rotation in megagauss fields over the continuous visible spectrum[J]. Rev Sci Instrum, 1968, 39(9): 1313–1317.

[32] TAMARU Y, CHEN H J, FUCHIMUKAI A, et al. Wavelength dependence of the Verdet constant in synthetic quartz glass for deep-ultraviolet light sources[J]. Opt Mater Express, 2021, 11(3): 814.

[33] YIN S Y, LOUSTEAU J, OLIVERO M, et al. Analysis of Faraday effect in multimode tellurite glass optical fiber for magneto-optical sensing and monitoring applications[J]. Appl Opt, 2012, 51(19): 4542–4546.

[34] YIN S Y, ZHANG Z Z, LI Y, et al. Faraday angle and accuracy measurement of magneto-optic current transmission based on new telluride glass[J]. IEEE Photonics J, 2022, 14(5): 6852706.

[35] ZHANG F, LI B, SUN Y, et al. A magnetic field sensor utilizing tellurite fiber-induced Sagnac loop based on faraday rotation effect and Fresnel reflection[J]. IEEE Trans Instrum Meas, 2021, 70: 7004407.

[36] KUROSAWA K, YOSHIDA S, SAKAMOTO K, et al. A current sensor using the Faraday effect in optical fiber manufactured from flint glass[J]. Electr Eng Jpn, 1997, 118(3): 22–38.

[37] CEASE T W, JOHNSTON P. A magneto-optic current transducer[J]. IEEE Trans Power Deliv, 1990, 5(2): 548–555.

[38] KANOE M, TAKAHASHI G, SATO T, et al. Optical voltage and current measuring system for electric power systems[J]. IEEE Trans Power Deliv, 1986, 1(1): 91–97.

[39] ROBINSON C C, GRAF R E. Faraday rotation in praseodymium, terbium, and dysprosium alumina silicate glasses[J]. Appl Opt, 1964, 3(10): 1190–1191.

[40] DAYBELL M, OVERTON W C Jr, LAQUER H L. The faraday effect at low temperatures in terbium alumina silicate glass[J]. Appl Phys Lett, 1967, 11(3): 79–81.

[41] PYE L D, CHERUKURI S C, MANSFIELD J, et al. The Faraday effect in some non-crystalline fluorides[J]. J Non Cryst Solids, 1983, 56(1–3): 99–104.

[42] YAMADA K, MATSUMOTO K, MARUYAMA F. Enhancement of faraday effect by resonance lines of rare earth oxide glass[J]. J Magn Soc Jpn, 1987, 11(S1): 269–272.

[43] LETELLIER V, SEIGNAC A, LE FLOCH A, et al. Magneto-optical properties of heavily rare-earth doped non-crystalline fluorophosphates[J]. J Non Cryst Solids, 1989, 111(1): 55–62.

[44] SHELBY J E, KOHLI J T. Rare-earth aluminosilicate glasses[J]. J Am Ceram Soc, 1990, 73(1): 39–42.

[45] PETROVSKII G T, EDELMAN I S, ZARUBINA T V, et al. Faraday effect and spectral properties of high-concentrated rare earth oxide glasses in visible and near UV region[J]. J Non Cryst Solids, 1991, 130(1): 35–40.

[46] ASAHARA Y. Glass and optical materials for lasers[J]. J Ceram Soc Japan, 1991, 99(1154): 903–911.

[47] BALLATO J, SNITZER E. Fabrication of fibers with high rare-earth concentrations for Faraday isolator applications[J]. Appl Opt, 1995, 34(30): 6848–6854.

[48] QIU J R, QIU J B, HIGUCHI H, et al. Faraday effect of $GaS_{3/2}$-GeS_2-$LaS_{3/2}$-based glasses containing various rare-earth ions[J]. J Appl Phys, 1996, 80(9): 5297–5300.

[49] LEE H G, WON Y H, LEE G S. Faraday rotation of Hoya FR5 glass at cryogenic temperature[J]. Appl Phys Lett, 1996, 68(22): 3072–3074.

[50] HAYAKAWA T, NOGAMI M, NISHI N, et al. Faraday rotation effect of highly Tb_2O_3/Dy_2O_3-concentrated B_2O_3−Ga_2O_3−SiO_2−P_2O_5 glasses[J]. Chem Mater, 2002, 14(8): 3223–3225.

[51] LI W N, ZOU K S, LU M, et al. Faraday glasses with a large size and high performance[J]. Int J Appl Ceram Technol, 2010, 7(3): 369–374.

[52] STAROBOR A, PALASHOV O, BABKINA A, et al. Magneto-optical properties of cerium-doped phosphate glass[J]. J Non Cryst Solids, 2019, 524: 119644.

[53] BELLANGER B, LEDEMI Y, MESSADDEQ Y. Fluorophosphate glasses with high terbium content for magneto-optical applications[J]. J Phys Chem C, 2020, 124(9): 5353–5362.

[54] BELLANGER B, AUDEBERT L, LEDEMI Y, et al. Superexchange interaction influence on the faraday effect in terbium fluorophosphate glasses by co-doping with praseodymium, dysprosium, and holmium[J]. J Phys Chem C, 2021, 125(31): 17482–17492.

[55] KANCHI S, SHUKLA R, DEY P, et al. Miniaturized double transit magnetic field measurement probe using the Faraday rotation principle[J]. Appl Opt, 2023, 62(4): 1123–1129.

[56] SUN L, JIANG S, MARCIANTE J R. All-fiber optical magnetic-field sensor based on Faraday rotation in highly terbium-doped fiber[J]. Opt Express, 2010, 18(6): 5407–5412.

[57] STAROBOR A V, ZHELEZNOV D S, PALASHOV O V, et al. Borogermanate glasses for Faraday isolators at high average power[J]. Opt Commun, 2016, 358: 176–179.

[58] BABKINA A, KULPINA E, SGIBNEV Y, et al. Terbium concentration effect on magneto-optical properties of ternary phosphate glass[J]. Opt Mater, 2020, 100: 109692.

[59] CHEN Q L, MA Q H. Mixed samarium valences effect in Faraday rotation glasses: Structure, optical, magnetic and magneto-optical properties[J]. J Non Cryst Solids, 2020, 530: 119803.

[60] LIN H, ZHOU L N, LIU B Y, et al. Research on the magneto-optical properties of Tb^{3+}-Ho^{3+} Co-doped GeO_2-B_2O_3-P_2O_5-ZnO (GBPZ) Faraday glass[J]. J Non Cryst Solids, 2022, 587: 121589.

[61] XIE J S, ZHANG M H, ZENG H C, et al. Tb_2O_3/Ce_2O_3-codoped B_2O_3–Ga_2O_3(Al_2O_3) glasses with a large faraday effect synthesized *via* containerless method for small optic isolators[J]. ACS Appl Mater Interfaces, 2025, 17(9): 14211–14219.

[62] TANAKA K, HIRAO K, SOGA N. Large Verdet constant of $30Tb_2O_3 \cdot 70B_2O_3$ glass[J]. Jpn J Appl Phys, 1995, 34(9R): 4825.

[63] QIU J R, TANAKA K, SUGIMOTO N, et al. Faraday effect in Tb^{3+}-containing borate, fluoride and fluorophosphate glasses[J]. J Non Cryst Solids, 1997, 213–214: 193–198.

[64] TANAKA K, FUJITA K, SOGA N, et al. Faraday effect of sodium borate glasses containing divalent europium ions[J]. J Appl Phys, 1997, 82(2): 840–844.

[65] QIU J R, TANAKA K, HIRAO K. Preparation and faraday effect of fluoroaluminate glasses containing divalent europium ions[J]. J Am Ceram Soc, 1997, 80(10): 2696–2698.

[66] TANAKA K, FUJITA K, MATSUOKA N, et al. Large Faraday effect and local structure of alkali silicate glasses containing divalent europium ions[J]. J Mater Res, 1998, 13(7): 1989–1995.

[67] TANAKA K, TATEHATA N, FUJITA K, et al. The Faraday effect and magneto-optical figure of merit in the visible region for lithium borate glasses containing[J]. J Phys D Appl Phys, 1998, 31(19): 2622.

[68] AKAMATSU H, FUJITA K, NAKATSUKA Y, et al. Magneto-optical properties of Eu^{2+}-containing aluminoborosilicate glasses with ferromagnetic interactions[J]. Opt Mater, 2013, 35(11): 1997–2000.

[69] SUZUKI F, SATO F, OSHITA H, et al. Large Faraday effect of borate glasses with high Tb^{3+} content prepared by containerless processing[J]. Opt Mater, 2018, 76: 174–177.

[70] ZHANG Y M, MURAI S, MAENO A, et al. Microstructure and Faraday effect of Tb_2O_3-Al_2O_3-SiO_2-B_2O_3 glasses for fiber-based magneto-optical applications[J]. J Am Ceram Soc, 2022, 105(2): 1198–1209.

[71] SASAKI S, TANAKA K, MASUNO A. Magneto-optical effect of rare-earth-rich borate glasses prepared using a levitation technique[J]. J Am Ceram Soc, 2024, 107(12): 8126–8131.

[72] JIA H J, ZHU Z L. Concentration-wavelength dependence of magneto-optical properties in Tb^{3+}-doped BGAP Glass[J]. J Non Cryst Solids, 2021, 552: 120456.

[73] HAN X X, KANG M H, FAN C L, et al. Formation and magneto-optical properties of Tb_2O_3-doped gallium borate glass[J]. J Non Cryst Solids, 2024, 639: 123108.

[74] ZHOU L N, ZHU Z L. Study of magneto-optical properties of GeO_2-B_2O_3-P_2O_5-ZnO-Tb_2O_3 glass doped with different rare-earth ions[J]. J Non Cryst Solids, 2022, 576: 121241.

[75] HAN X X, LIU C, NIU L Y, et al. Tb^{3+}-doped fluoro-borosilicate magneto-optical glass with a large Verdet constant for current sensing[J]. Ceram Int, 2025, 51(1): 1096–1102.

[76] LIU B Y, ZHU Z L. The effect of Tb^{3+} on magneto-optical properties of GeO_2-B_2O_3-Li_2O-MgO glasses[J]. J Non Cryst Solids, 2023, 609: 122265.

[77] LIN H, YANG H H, ZHOU L N, et al. Research on the physical and optical properties of Dy^{3+} doped 30 mol%Tb_2O_3–B_2O_3-GeO_2-PbO-SiO_2 magneto-optical glass with high Verdet constant[J]. J Phys Chem Solids, 2022, 166: 110682.

[78] ZHAO X D, LI J D, LI W W, et al. Magneto-optical and luminescent properties of Tb doped Ge-B-X (X=Ga/La) glasses[J]. Ceram Int, 2024, 50(9): 16663–16671.

[79] ZHOU L N, ZHU Z L. Magneto-optical and luminescent properties of Tb^{3+} ions doped GBPZ magneto-optical glass[J]. J Non Cryst Solids, 2021, 574: 121165.

[80] DUBROVIN V D, ZHU X, MOLLAEE M, et al. Highly Dy_2O_3 and Er_2O_3 doped boron-aluminosilicate glasses for magneto-optical devices operating at 2 μm[J]. J Non Cryst Solids, 2021, 569: 120986.

[81] ALZAHRANI J S, ALROWAILI Z A, EKE C, et al. Tb^{3+}-doped GeO_2-B_2O_3–P_2O_5–ZnO magneto-optical glasses: Potential application as gamma-radiation absorbers[J]. Radiat Phys Chem, 2023, 208: 110874.

[82] ROSOLEM J B, FLORIDIA C, BASSAN F R, et al. Performance of Tb glass used to fabricate special optical fiber as a discrete current sensor[C]//2023 SBMO/IEEE MTT-S International Microwave and Optoelectronics Conference (IMOC). Castelldefels, Spain. IEEE, 2023: 40–42.

[83] ZHAO X D, LI W W, XIA Q, et al. High Verdet constant glass for magnetic field sensors[J]. ACS Appl Mater Interfaces, 2022, 14(51): 57028–57036.

[84] SANTOS S N C, ROMERO A L S, MENEZES B C, et al. Femtosecond-laser fabrication of magneto-optical waveguides in terbium doped CaLiBO glass[J]. Opt Mater, 2022, 126: 112197.

[85] FRANCO D F, LEDEMI Y, CORRER W, et al. Magneto-optical borogermanate glasses and fibers containing Tb^{3+} [J]. Sci Rep, 2021, 11(1): 9906.

[86] YANG H H, ZHU Z L. Magneto-optical glass mixed with Tb^{3+} ions: High Verdet constant and luminescence properties[J]. J Lumin, 2021, 231: 117804.

[87] LIN H, LIU B Y, ZHOU L N, et al. Enhancements of magneto-optical properties of GeO_2-PbO-B_2O_3–SiO_2–P_2O_5 glass doped Tb^{3+} ion[J]. Mater Chem Phys, 2022, 282: 125963.

[88] LINGANNA K, RYU Y, NAEEM K, et al. Fabrication and characterization of highly Dy^{3+}- and Tb^{3+}-doped germano-borate glasses for magneto-optic device applications at 1.55 μm[J]. J Non Cryst Solids, 2022, 585: 121520.

[89] HAO C H, ZHU Z L. The effect of trace Fe^{3+} on the magneto-optical properties of Tb^{3+} doped B_2O_3-GeO_2-Al_2O_3-ZnO-BaO glass[J]. Opt Mater, 2024, 154: 115706.

[90] LI J D, ZHAO X D, LI W W, et al. Effect of Na_2O on Verdet constant of Tb-doped magneto-optical glass[J]. Opt Mater, 2024, 151: 115388.

[91] LIN H, LI G F, HAO C H, et al. Study on the physical properties and luminescent properties of Tb^{3+}doped GBBS magneto-optical glass[J]. Opt Mater, 2024, 150: 115072.

[92] ALBINO L V, DUSSAUZE M, TOULEMONDE O, et al. Paramagnetic borotungstate glasses with high terbium concentration for magneto-optical applications[J]. J Non Cryst Solids, 2024, 627: 122811.

[93] LI J D, ZHAO X D, CHANG Y X, et al. High Verdet constant of Tb_2O_3-doped TiO-B_2O_3-Al_2O_3-Na_2O magneto-optical glass[J]. Opt Express, 2024, 32(9): 16506–16513.

[94] ZHAO X D, LI J D, LI W W, et al. Valence state regulation of Terbium in all-inorganic amorphous solid for magnetic field sensing[J]. Chem Eng J, 2024, 488: 150898.

[95] HAN X X, HU W P, ZHENG X X, et al. Effects of temperature on magneto-optical properties of high terbium fluoro-oxide glass[J]. Opt Mater, 2025, 166: 117215.

[96] VAN VLECK J H, HEBB M H. On the paramagnetic rotation of tysonite[J]. Phys Rev, 1934, 46(1): 17–32.

[97] DUFFY J A, INGRAM M D. Establishment of an optical scale for Lewis basicity in inorganic oxyacids, molten salts, and glasses[J]. J Am Chem Soc, 1971, 93(24): 6448–6454.

[98] DUFFY J A, INGRAM M D. An interpretation of glass chemistry in terms of the optical basicity concept[J]. J Non Cryst Solids, 1976, 21(3): 373–410.

[99] PRICE D L. High-temperature levitated materials[M]. Cambridge, New York: Cambridge University Press, 2010.

[100] MASUNO A. Functionalities in unconventional oxide glasses prepared using a levitation technique[J]. J Ceram Soc Japan, 2022, 130(8): 563–574.

[101] YOSHIMOTO K, MASUNO A, UEDA M, et al. Low phonon energies and wideband optical windows of La_2O_3-Ga_2O_3 glasses prepared using an aerodynamic levitation technique[J]. Sci Rep, 2017, 7: 45600.

[102] YOSHIMOTO K, EZURA Y, UEDA M, et al. 2.7 μm mid-infrared emission in highly erbium-doped lanthanum gallate glasses prepared *via* an aerodynamic levitation technique[J]. Adv Opt Mater, 2018, 6(8): 1701283.

[103] SUZUKI F, FURUYAMA T, SATO F, et al. Faraday isolators for high-power lasers using magneto-optical glass[C]//Components and Packaging for Laser Systems XI. San Francisco, USA. SPIE, 2025: 21.

[104] CANNELLA V, MYDOSH J A. Magnetic ordering in gold-iron alloys[J]. Phys Rev B, 1972, 6(11): 4220–4237.

[105] EDWARDS S F, ANDERSON P W. Theory of spin glasses[J]. J Phys F: Metal Phys, 1975, 5(5): 965.

[106] The following are Nobel prize winners who greatly contributed to the advancement of spin glass theory and its application: P. W. Andrson (1977), D. J. Thouless (2016), G. Parisi (2021), J. Hopfield (2024).

[107] VERHELST R A, KLINE R W, DE GRAAT A M, et al. Magnetic properties of cobalt and manganese aluminosilicate glasses[J]. Phys Rev B, 1975, 11(11): 4427–4435.

[108] RECHENBERG H R, BIEMAN L H, HUANG F S, et al. Remanent magnetization of $CoO \cdot Al_2O_3 \cdot SiO_2$ glass: A log*t* law[J]. J Appl Phys, 1978, 49(3): 1638–1639.

[109] SANCHEZ J P, FRIEDT J M, HORNE R, et al. Spin glass transition and hyperfine parameters in FeO-Al_2O_3-SiO_2 glasses[J]. J Phys C Solid State Phys, 1984, 17(1): 127.

[110] SHAW J L, WRIGHT A C, SINCLAIR R N, et al. Spin glass-like antiferromagnetic interactions in iron phosphate glasses[J]. J Non

Cryst Solids, 2004, 345: 245–250.

[111] RENARD J P, MIRANDAY J P, VARRET F. Evidence of a spin-glass transition in the vitrous insulating flourides “$PbMnFeF_7$” and “Pb_2MnFeF_9”[J]. Solid State Commun, 1980, 35(1): 41–44.

[112] AKAMATSU H, TANAKA K, FUJITA K, et al. Spin dynamics in Fe_2O_3–TeO_2 glass: Experimental evidence for an amorphous oxide spin glass[J]. Phys Rev B, 2006, 74: 012411.

[113] AKAMATSU H, TANAKA K, FUJITA K, et al. Spin dynamics in oxide glass of Fe_2O_3–Bi_2O_3–B_2O_3 system[J]. J Magn Magn Mater, 2007, 310(2): 1506–1507.

[114] AKAMATSU H, TANAKA K, FUJITA K, et al. Magnetic phase transitions in Fe_2O_3–Bi_2O_3–B_2O_3[J]. J Phys Condens Matter, 2008, 20(23): 235216.

[115] AKAMATSU H, OKU S, FUJITA K, et al. Magnetic properties of mixed-valence iron phosphate glasses[J]. Phys Rev B, 2009, 80(13): 134408.

[116] AKAMATSU H, KAWABATA J, FUJITA K, et al. Magnetic properties of oxide glasses containing iron and rare-earth ions[J]. Phys Rev B, 2011, 84(14): 144408.

[117] SCHOENES J, KALDIS E, THÖNI W, et al. Optical, magnetic, and magnetooptical properties of the europium silicate glass $Eu_{0.14}Si_{0.31}O_{0.55}$[J]. Phys Status Solidi A, 1979, 51(1): 173–181.

[118] AKAMATSU H, FUJITA K, MURAI S, et al. Ferromagnetic Eu^{2+}-based oxide glasses with reentrant spin glass behavior[J]. Phys Rev B, 2010, 81: 014423.

[119] AKAMATSU H, FUJITA K, ZONG Y H, et al. Impact of amorphization on the magnetic properties of EuO-TiO_2 system[J]. Phys Rev B, 2010, 82(22): 224403.

[120] KATSUFUJI T, TAKAGI H. Coupling between magnetism and dielectric properties in quantum paraelectric $EuTiO_3$[J]. Phys Rev B, 2001, 64(5): 054415.

[121] CHIEN C-L, DEBENEDETTI S, BARROS F D S. Magnetic properties of $EuTiO_3$, Eu_2TiO_4, and $Eu_3Ti_2O_7$[J]. Phys Rev B. 1974, 10(9): 3913–3922.

[122] PAUTHENET R. Magnetic properties of the rare earth garnets[J]. J Appl Phys, 1959, 30(4): S290–S292.

[123] GYORGY E M, NASSAU K, NASSAU K, et al. The magnetic properties of amorphous $Y_3Fe_5O_{12}$[J]. J Appl Phys, 1979, 50(4): 2883–2886.

[124] MOREAU J M, MICHEL C, GERSON R, et al. Ferroelectric $BiFeO_3$ X-ray and neutron diffraction study[J]. J Phys Chem Solids, 1971, 32(6): 1315–1320.

[125] NAKAMURA S, SOEYA S, IKEDA N, et al. Spin-glass behavior in amorphous $BiFeO_3$[J]. J Appl Phys, 1993, 74(9): 5652–5657.

[126] ZONG Y H, FUJITA K, AKAMATSU H, et al. Local structure of amorphous EuO–TiO_2 thin films probed by X-ray absorption fine structure[J]. J Am Ceram Soc, 2012, 95(2): 716–720.

[127] KAWAMOTO T, FUJITA K, AKAMATSU H, et al. Ferromagnetic amorphous oxides in the EuO-TiO_2 system studied by the Faraday effect in the visible region and the X-ray magnetic circular dichroism at the $EuM_{4,5}$ and $L_{2,3}$ edges[J]. Phys Rev B, 2013, 88(2): 024405.

[128] SUITS J C, ARGYLE B E. Paramagnetic faraday rotation of EuSe[J]. J Appl Phys, 1965, 36(3): 1251–1252.

[129] POMMIER J, FERRE J, SENOUSSI S. Origin of the Faraday effect in a transparent magnetic Mn^{2+} glass[J]. J Phys C Solid State Phys, 1984, 17(31): 5621–5633.

[130] IMAIZUMI D, HAYAKAWA T, NOGAMI M. Faraday rotation effects of Mn^{2+}-modified Tb_2O_3-B_2O_3 glass in pulsed magnetic field[J]. J Light Technol, 2002, 20(4): 740–744.

[131] IVANOVA O S, PETRAKOVSKAYA É A, IVANTSOV R D, et al. Effect of heat treatment and concentration of Mn and Fe on the structure of borate glass[J]. J Appl Spectrosc, 2006, 73(3): 400–405.

[132] WINTERSTEIN A, AKAMATSU H, MÖNCKE D, et al. Magnetic and magneto-optical quenching in (Mn^{2+}, Sr^{2+}) metaphosphate glasses[J]. Opt Mater Express, 2013, 3(2): 184.

[133] ALBINO L V, ROQUE N G, MARCONDES L M, et al. Magnetic and magneto-optical properties of manganese-containing antimony phosphate glasses–An alternative to Faraday rotators[J]. Opt Mater, 2024, 147: 114674.

[134] AKAMATSU H, FUJITA K, MURAI S, et al. Magneto-optical properties of transparent divalent iron phosphate glasses[J]. Appl Phys Lett, 2008, 92(25): 251908.

[135] YU J B, GU Y, ZHANG Q, et al. A new type of NiO-doped phosphate glass with excellent Faraday effects[J]. Mater Lett, 2018, 212: 25–27.

[136] NAKATSUKA Y, POLLOK K, WIEDUWILT T, et al. Giant faraday rotation through ultrasmall Fe^0_n clusters in superparamagnetic FeO-SiO_2 vitreous films[J]. Adv Sci, 2017, 4(4): 1600299.

[137] CHEN Q L, LI Z Z, MIAO B J. Giant Faraday rotation, magnetic and nonlinearity of diamagnetic glass tailored by plasmonic-magnetic bimetallic Au-Ni NPs[J]. J Alloys Compd, 2022, 900: 163536.

[138] NAKASHIMA S, SUGIOKA K, MIDORIKAWA K, et al. Spatially selective modification of optical and magneto-optical properties in Fe- and Au-doped glasses irradiated with femtosecond-laser[J]. Appl Phys A, 2013, 110(4): 765–769.

[139] NAKASHIMA S. Plasmonically coupled faraday effect in Fe- and Au-doped silicate glasses irradiated with femtosecond laser[J]. J Laser Micro, 2014, 9(2): 132–136.

[140] NAKASHIMA S, OKABE R, SUGIOKA K, et al. Fabrication of magneto-optical waveguides inside transparent silica xerogels containing ferrimagnetic Fe_3O_4 nanoparticles[J]. Opt Express, 2018, 26(24): 31898–31907.

[141] CHEN Q L, FAN J H, MIAO B J, et al. Spinel ferrites $NiFe_2O_4$ NCs enhanced Mössbauer spectra, magnetization and Faraday rotation of diamagnetic tellurite glasses[J]. Ceram Int, 2022, 48(20): 30191–30205.

[142] CHEN Q L, CHEN W H. Magnetic and magneto-optical properties of $La_{0.8}Sr_{0.2}FeO_3$ crystals in alumina doped lead-bismuth-borate Faraday rotating glass matrix[J]. J Non Cryst Solids, 2022, 595: 121807.

[143] CHEN Q L, LI Z Z, CHEN W H. Structural, optical, magnetic and Faraday rotation properties of $MnSe_2$: Eu doped diamagnetic materials: The impact of multi-valence states of Mn and Eu[J]. J Alloys Compd, 2021, 872: 159655.

[144] WANG S, CHEN Q L. Al_2O_3 triggered *in situ* crystallization of $Gd_3Al_2Ga_3O_{12}$ in glass and enhancement in magnetic and Faraday rotating properties[J]. J Eur Ceram Soc, 2023, 43(8): 3572–3590.

[145] SHI H, WEN J X, XING B B, et al. Polarization and magneto-optical characteristics of Tb: YAG crystal-derived silica fiber *via* laser-heating drawing technique[J]. Chin Opt Lett, 2023, 21(11): 110601.

[146] BELLANGER B, CORRER W, VÉRON E, et al. Structural environment influence on Faraday effect in Tb^{3+} and Pr^{3+} co-doped fluorophosphate glass and glass-ceramics containing TbOF nanocrystals[J].

J Alloys Compd, 2023, 960: 170715.

[147] CHEN Q L, CHEN W H, LI Z Z, et al. Mixed valence effects in $TbVO_4$: Y nanocrystals and diamagnetic materials: Structure, optical linear & nonlinear, magnetic and Faraday rotation properties[J]. J Alloys Compd, 2021, 867: 159065.

[148] ZHANG X H, CHEN Q L, ZHANG S H. Mixed valence effects in Pr: YbF_3 nanocrystals and influence to EPR, magnetic and Faraday rotation properties of diamagnetic glasses[J]. J Non Cryst Solids, 2021, 572: 121112.

[149] CHEN Q L, LI Z Z, MIAO B J, et al. Thermal, nonlinear, magnetic and faraday rotation properties of sol-gel diamagnetic glass/$NaYF_4$: Fe, Ho^{3+}: Role of magnetic ions[J]. J Alloys Compd, 2021, 858: 157631.

[150] LIN H, JIA H J, ZHOU L N, et al. Magneto-optical and fluorescence properties of Tb^{3+} doped glass-ceramics containing $AlPO_4$[J]. J Non Cryst Solids, 2022, 579: 121377.

[151] CHEN Q, LI Z, MIAO B, et al. Ta_2O_5 nanocrystals strengthened linear, nonlinear, and Faraday properties of heavy metal oxide diamagnetic material[J]. J Am Ceram Soc. 105(1): 225–244.

[152] MIAO B J, CHEN Q L, CHEN W H. The role of 4f14 Lu^{3+} and 3d0 Sc^{3+} in faraday rotating glass/ceramic: Structural stability, magnetic and magneto optical properties[J]. Ceram Int, 2022, 48(9): 12193–12208.

[153] HIGASHINO M, MURAI S, LO T Y, et al. Photoluminescence coupled to electric and magnetic surface lattice resonance in periodic arrays of zirconia nanoparticles[J]. J Mater Chem C, 2022, 10(26): 9730–9739.

[154] MURAI S, ZHANG F F, AICHI K, et al. Photoluminescence engineering with nanoantenna phosphors[J]. J Mater Chem C, 2023, 11(2): 472–479.

[155] MURAI S, MARUYAMA H, TSE J T Y, et al. Mechanically reconfigurable silicon carbide metasurface stickers[J]. ACS Appl Opt Mater, 2025, 3(9): 2006–2012.

作者贡献声明：

TANAKA Katsuhisa：提出研究方向，设计论文框架并撰写稿件，完善论文框架并修改稿件。

Recent Development on Oxide Glasses Exhibiting the Faraday Effect

TANAKA Katsuhisa

(Department of Material Chemistry, Graduate School of Engineering, Kyoto University, Nishikyo-ku, Kyoto 615-8510, Japan)

Extended Abstract

The Faraday effect is one of the magneto-optical phenomena and refers to the conversion of linearly polarized light passing through a magnetic material into elliptically polarized light with the main axis–containing polarization plane rotated around the propagation vector. The angle by which the polarization plane is rotated, *i.e.*, the Faraday rotation angle, is an important parameter determining the applicability of magnetic materials in devices such as electric-current and magnetic-field sensors, optical isolators, and optical circulators. Since the Faraday effect deals with a transmitted light, the transmittance of the magnetic materials is another important factor for applications. Thus, the materials are required to show a great magneto-optical figure of merit, that is defined as Faraday rotation angle or Verdet constant divided by absorbance or optical absorption coefficient. Here, the Verdet constant is defined as the Faraday rotation angle divided by external magnetic field and light path length inside the magnetic materials. It is well known that single crystals of garnet-type ferrites such as $Y_3Fe_5O_{12}$ and $(Gd,Bi)_3Fe_5O_{12}$ exhibit a large Faraday effect and a low optical absorption in the infrared region, especially in a wavelength range from 1.3 μm to 1.5 μm, and that they are effectively utilized as an optical isolator for optical telecommunications. However, compared to the garnet-type ferrites in the infrared region, magneto-optical materials with the superior performance, are lacking in the visible to ultraviolet region. Hence, the development of such materials is still in progress.

Oxide glasses rich in rare-earth ions exhibit a great Faraday effect, especially in the visible to ultraviolet range. Although these glasses feature magnetizations smaller than those of ferro- or ferri-magnetic oxide crystals such as abovementioned $Y_3Fe_5O_{12}$ because the rare-earth-containing glasses are usually paramagnetic at room temperature, the transmittance of these glasses notably exceeds that of ferrite crystals in the visible to ultraviolet range. In addition, oxide glass has an advantage that it is feasible to tune continuously the composition so that optimized properties are attained and to fabricate large-sized and specific-shaped materials. In addition to the paramagnetic glasses, the Faraday effect of diamagnetic glasses is intensively investigated as well. The magnetization of diamagnetic glasses is further smaller than that of paramagnetic glasses, but the Faraday rotation angle or the Verdet constant of diamagnetic glasses is almost independent of temperature. This is an advantageous point of diamagnetic glasses, which cannot be realized in ferro-magnetic, ferri-magnetic, and para-magnetic materials. Furthermore, for wide-band gap oxide glass like SiO_2 glass, which is diamagnetic, the Faraday effect can occur even in a very short wavelength range such as the deep and vacuum ultraviolet.

This review represents recent development on oxide glasses exhibiting large Faraday rotation. The macroscopic and microscopic mechanism of the Faraday effect are explained. The microscopic mechanism is very important to select magneto-optically active elements and to design glass compositions.Also, the Faraday effect of diamagnetic glasses is described. Heavy-metal oxide glasses and sulfide glasses are intensely exploited because the magnetic susceptibility of diamagnetic materials depends on the constituent atoms (ions) and the susceptibility is proportional to the squared atomic (ionic) radius and the number of electrons contained in the atom (ion). The Verdet constants of these glasses are summarized. The applications of diamagnetic glasses are briefly mentioned.

Subsequently, the Faraday effect of paramagnetic oxide glasses containing large amounts of rare-earth ions is reviewed. The pioneering work in this field has been carried out in the mid-1960s, showing that some ions like Ce^{3+}, Pr^{3+}, Tb^{3+}, Dy^{3+}, and Eu^{2+} give rise to larger Verdet constants in the visible range. A description is given to explain why these rare-earth ions exhibit larger Faraday effects than other ones. Recent researches seem to mainly pay attention to Tb^{3+}-rich oxide glasses, for which higher concentrations of Tb^{3+} ions simply enhance the Verdet constant. In particular, Tb^{3+}-rich oxide glasses fabricated *via* containerless processing, which is an emerging method and effective to expand the glass-forming region, showing the larger Verdet constant than single-crystalline $Tb_3Ga_5O_{12}$ used as a commercially available optical isolator in the visible range. Furthermore, EuO-based amorphous oxides that have an unexpected ferromagnetism exhibit rather large Faraday effect.

In addition to the abovementioned diamagnetic oxide glasses and rare-earth-rich oxide glasses, a brief review concerns the Faraday effect of oxide glasses containing large amounts of 3d transition metal ions as well as glass-ceramics comprising ferro- or ferri-magnetic nano-sized crystalline particles embedded in transparent glass matrices.

Summary and Prospects The Faraday effect was discovered 180 years ago, but this phenomenon has been still utilized for practical applications as mentioned above. In particular, Tb^{3+}-rich and Eu^{2+}-rich oxide glasses are important for both fundamentals and applications. The Tb^{3+}-rich glasses show a high transparency even in blue to ultraviolet region, so that the magneto-optical figure of merit is large enough to apply for an optical isolator. The Eu^{2+}-rich glasses are ferromagnetic, so that they notably show a large Faraday effect. A new technique of glass formation such as containerless processing is effective to produce new glass compositions with further higher concentrations of rare-earth ions that are expected to exhibit a larger Verdet constant. Besides, the possible enhancement of Faraday effect based on plasmonics and Mie-tronics, *i.e.*, the usage of localized surface plasmon resonance of metal nanoparticles and the Mie resonance of dielectric nanoparticles to increase the Verdet constant, becomes an important subject in the near future. With the development of high-power lasers, the demand for optical isolators that can operate in a wide wavelength range must increase. The oxide glasses have a promising application in such fields.

Keywords oxide glass; Faraday effect; Verdet constant; ferromagnetic amorphous oxide; rare earth; divalent europium